doi:10.1038/nature12071

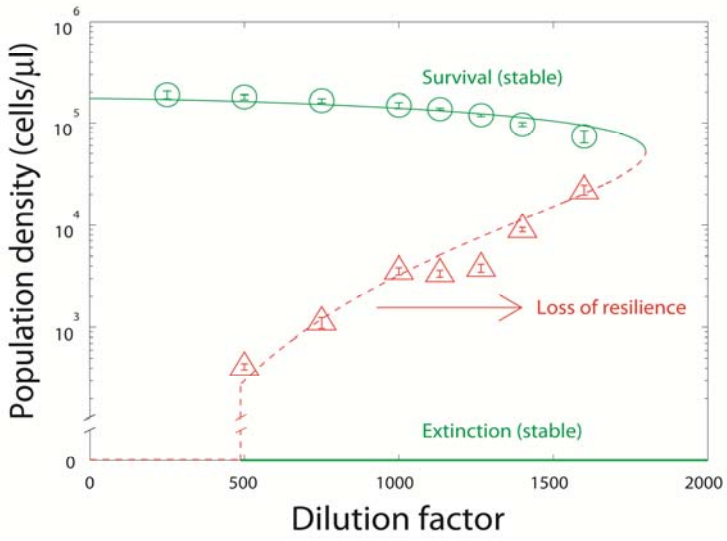

Supplementary Figure 1. Cooperative growth of yeast in sucrose leads to bistability and a fold bifurcation. Yeast cells grow cooperatively in sucrose by sharing the hydrolysis products[26]; this cooperative breakdown of sucrose makes the per capita growth rate of yeast ~40% higher at intermediate cell densities than at low cell densities[6]. It is a well characterized experimental system that displays a strong Allee effect[34] under daily dilutions[6]. During the daily dilution, only a small fraction (*e.g.* 1 in 500, for dilution factor 500) of the population is transferred to the fresh media. This is equivalent to introducing a mortality rate and leads to a negative growth rate at low initial cell densities. Therefore, cultures starting below a critical density go extinct, whereas cultures starting at higher initial densities survive and reach a finite stable fixed point. At intermediate dilution factors, yeast populations are bistable, with one stable fixed point at a finite population density and the other at extinction. A fold bifurcation occurs where the stable and unstable fixed points "collide" and annihilate. Increasing the dilution factor lowers the resilience of yeast populations and eventually pushes them to collapse after crossing the fold bifurcation (i.e. a tipping point). The data for this figure is taken from Reference 6. The stable fixed points are estimated by the mean of at least 46 replicate populations at equilibrium over 5 days and the error bars correspond to the standard deviation of day-to-day fluctuations. More details on the fitting of unstable fixed points and the error bars given by bootstrap can be found in the Supplementary Information of Reference 6.

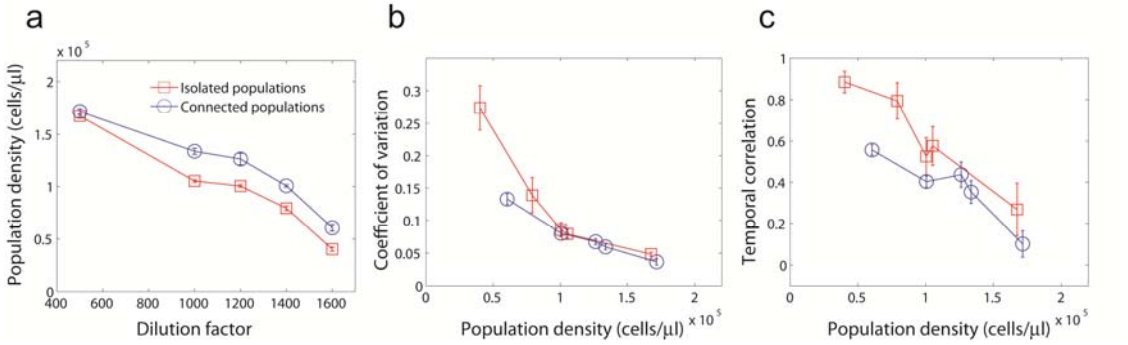

Supplementary Figure 2. The difference in coefficient of variation and temporal correlation between isolated and connected population may be partly due to a minor shift in bifurcation. (a) There is a small difference in the equilibrium density between the two groups of isolated and connected populations. The difference can be caused by small variation in experimental conditions (e.g. ~1% difference in the grow rate); it may also reflect a real difference due to some influence of spatial coupling on the stability landscape. Error bars are standard errors of day-to-day variations. (b, c) Because the difference in the equilibrium density may imply a minor shift in the bifurcation, we plot the warning indicators versus equilibrium population density (note that lower population density corresponds to higher dilution factor); this corrects the possible shift in the bifurcation to some extent. After correction we find that the increases of CV and temporal correlation in connected populations are still smaller than those in isolated populations. Error bars are SEs given by bootstrap for isolated populations and SEMs (n=4) for connected populations.

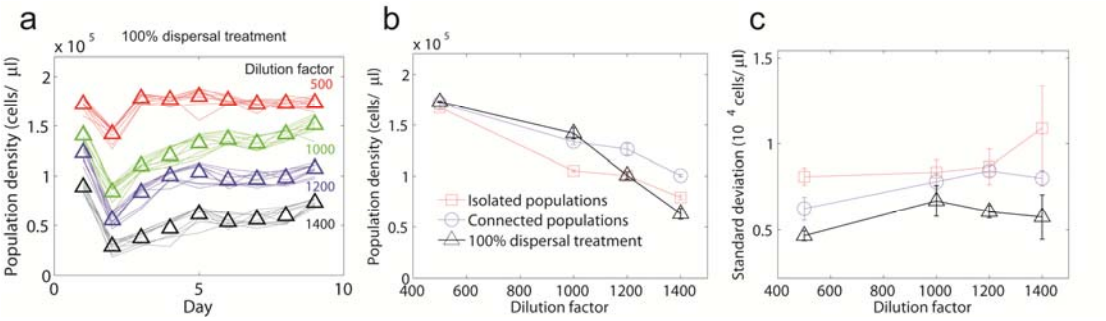

Supplementary Figure 3. The size of fluctuations is suppressed in populations with 100% dispersal treatment. (a) For each dilution factor (500, 1000, 1200 and 1400), there are 10 populations going through the "100% dispersal treatment". On each day, the 10 populations are mixed completely during the dispersal step. The triangle denotes the mean of 10 populations. Populations recovered from a "2x dilution shock" on day 2; there is a clear increase of recovery time with dilution factor, as a result of critical slowing down. (b) The mean equilibrium density of three experimental groups. The difference in mean population density between different groups may be due to variation in experimental conditions or the influence of spatial coupling; correcting the difference does not change the trend in indicators (Supplementary Figure 2). (c) The standard deviation of population fluctuations is reduced by dispersal. The standard deviation is calculated among 10 populations with 100% dispersal treatment over the last 3 days; the error bars are standard errors of day-to-day variations. The data used in Figure 2 for isolated and connected populations are plotted in light red and light blue. Temporal correlation is also expected to be suppressed (Supplementary Note 1 and Supplementary Figure 4). However, we are not able to get a reliable estimate of temporal correlation from the data of 100% dispersal treatment group because: 1) the sample size is too small; 2) populations have not fully reached equilibrium by the end of experiment, which also means it is difficult to remove gradient-type heterogeneity before statistical analysis (Methods).

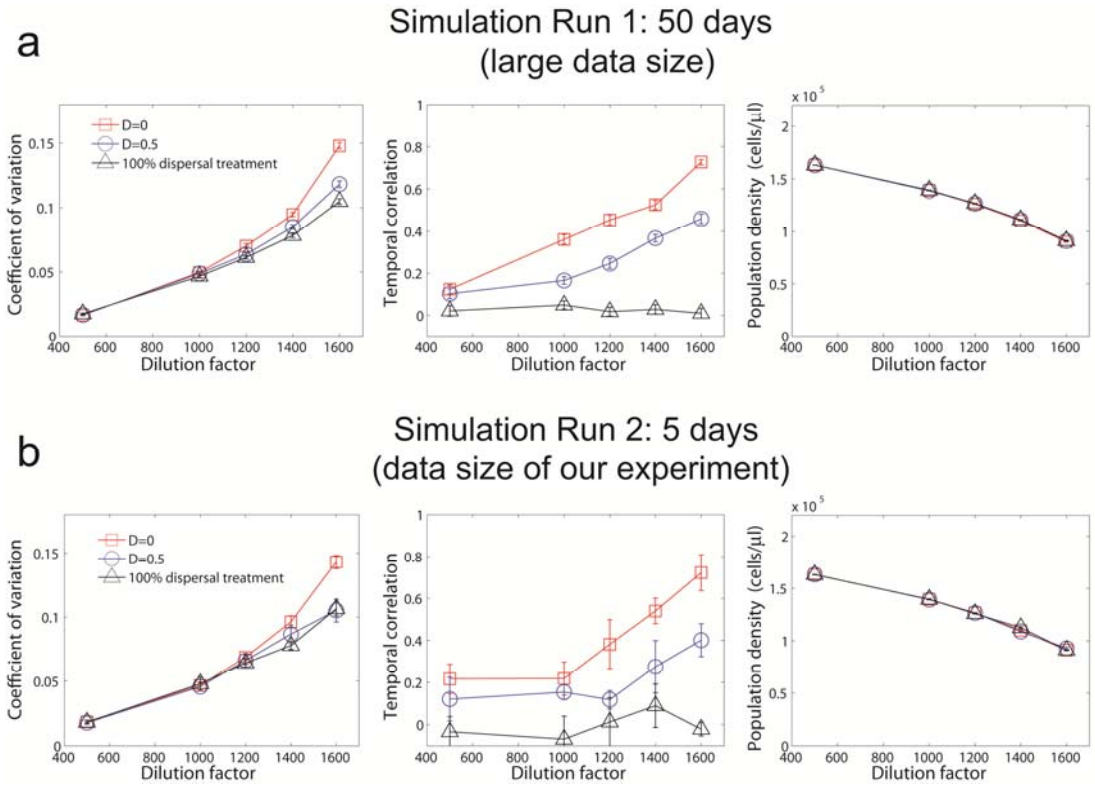

Supplementary Figure 4. Stochastic simulations based on a phenomenological model of yeast growth show that increases in coefficient of variation and temporal correlation are suppressed by population dispersal. For each dilution factor, there are 40 populations on a one-dimensional lattice. In the two simulation runs, the indicators are calculated over a span of 50 days **(a)** and 5 days **(b)** after an initial period of 10 days to stabilize the populations. Error bars are standard errors of day-to-day variations (n=50 for **a** and n=5 for **b**, respectively). The phenomenological model of yeast growth is briefly outlined in the following paragraph. More details of stochastic simulations can be found in the Supplementary Information of Reference 6. Dispersal rules in simulations are the same as those used in our experimental protocols.

The phenomenological model of yeast growth is based on two phases: a slow exponential growth phase at low cell densities, followed by a logistic growth phase with a higher per capita growth rate at intermediate cell densities. This model has five parameters: T_{lag} is the lag time before yeast cells start to grow after being transferred into new media. In the slow exponential phase, the population grows with a constant per capita growth rate γ_{low}.

After the population reaches a threshold density N_c, the subsequent logistic growth is determined by γ_{high} ($\gamma_{high}>\gamma_{low}$) and the carrying capacity K.

$$\frac{1}{N}\frac{dN}{dt}=\begin{cases}\gamma_{low} & 0<N<N_c\\ \gamma_{high}(1-\frac{N}{K}) & N_c\le N<K\end{cases} \qquad (1)$$

In the simulations, we used the parameter values listed in Supplementary Table 1. They are chosen as the values used in fitting an experimental fold bifurcation of this system[6].

We note that the exact values of equilibrium population density and statistical indicators in our simulations do not match perfectly with the experimental data. This is expected because: 1) our two-phase yeast growth model is an obvious simplification; 2) we only have crude estimates of the location of bifurcation and the magnitude of noise.

Supplementary Table 1. Parameters of a phenomenological model of yeast growth used in the simulations.

Parameter	Value
γ_{high}	0.439 hr^{-1}
γ_{low}	0.309 hr^{-1}
K	1.76×10^5 cells/μl
T_{lag}	2.97 hr
N_c	2.76×10^2 cells/μl

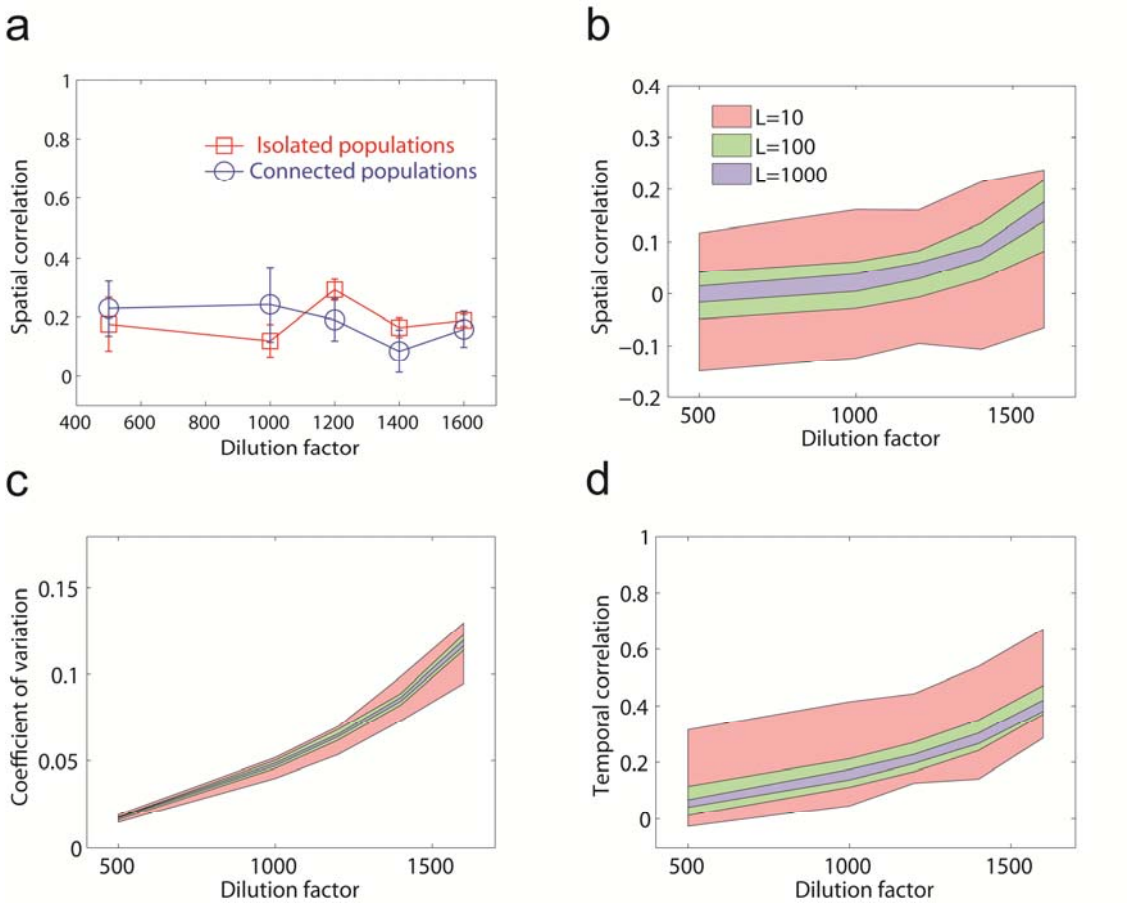

Supplementary Figure 5. Our experiment and simulations suggest that large sample sizes are required to observe an increase in spatial correlation. (a) We tested the two-point correlation between nearest neighbors in the connected populations but failed to observe any increase near the tipping point. The spatial correlation, defined as the two-point correlation between all neighboring pairs, was estimated by the Moran's coefficient[8,32] (Methods). Error bars are SEs given by bootstrap for isolated populations and SEMs (n=4) for connected populations. (b) In simulations, a statistically significant increase of spatial correlation is observed in connected populations given a large sample size (L is the number of populations on a one dimensional array). In our experiment, we have 4 replicate arrays with L=10 in each array. (c,d) Given the same sample size, coefficient of variation and temporal correlation are better warning indicators than spatial correlation in simulations. Thus, our results suggest that to observe the increase in spatial correlation may require more data than other indicators; nonetheless it can be a useful warning indicator in spatial data sets with very large sample sizes.

Stochastic simulations are performed in the same procedure as described in Supplementary Figure 4 (at dilution factors 500, 1000, 1200, 1400 and 1600; D=0.5). Indicators are calculated over a span of 5 days after an initial period of 10 days to stabilize the populations. The colored regions correspond to 16%-84% confidence interval of 100 simulation runs and can be asymmetric. We note that the values of indicators in simulation are not directly comparable to experimental data (Supplementary Figure 4). We also note that the indicators here are calculated based on an ensemble of replicates at a fixed condition. The performance of indicators based on detrended temporal fluctuations of a single population may be worse[35] because: 1) in a changing environment, temporal fluctuations are averaged over different environmental conditions; 2) the sample size is reduced by temporal correlation.

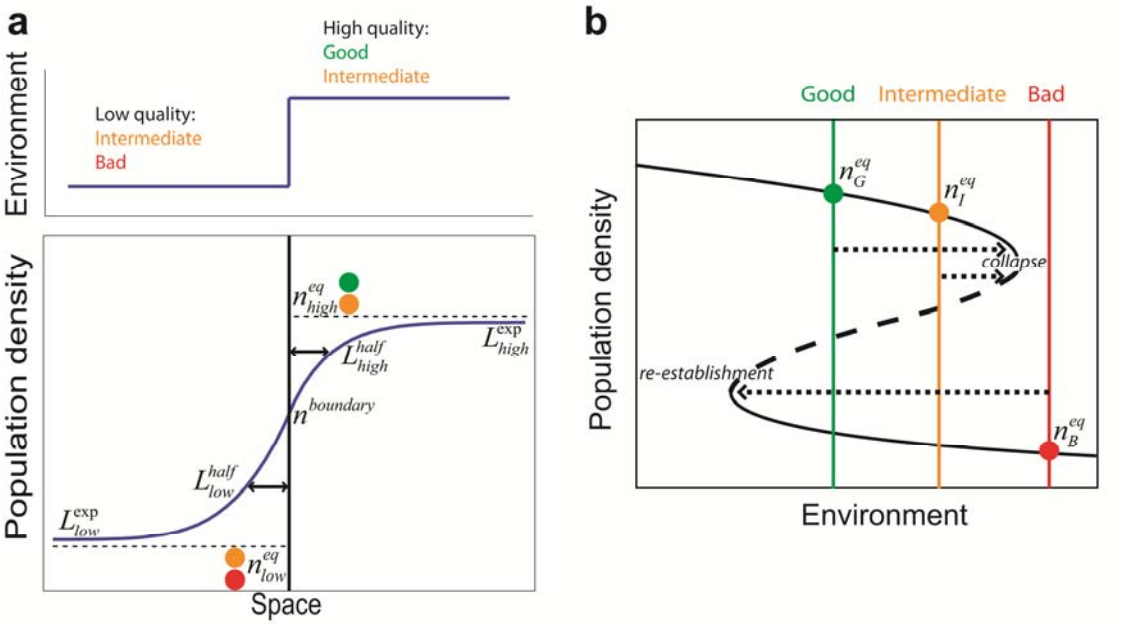

Supplementary Figure 6. Recovery length can be measured given a sharp boundary between two regions of different quality. (a) On both sides of the sharp boundary, population density is varying across the region. In each region, population density recovers from $n^{boundary} \equiv n(x=0)$ to the equilibrium n^{eq} of the corresponding environmental condition. One can quantify the spatial scale of recovery by: 1) half-point recovery length L^{half}, $n(x=L^{half}) = \frac{1}{2}(n^{eq} + n^{boundary})$; or 2) exponential recovery length $L^{\exp}$, $|n^{eq} - n(x)| = |n^{eq} - n^{boundary}|e^{-|x|/L^{\exp}}$ (Supplementary Note 2 and Methods). (b) The recovery length in each region indicates how far away its environmental condition is from the relevant bifurcation point (dashed arrows). The recovery rate is smaller closer to the bifurcation point, thus leading to longer recovery length (Supplementary Note 2). Typically we are interested in predicting impending collapse of the high-quality region (good or intermediate), so we designed the experiment in Figure 4 to measure L_{high}. An example to measure the recovery length in the low-quality region L_{low} is shown in Supplementary Figure 8. However, we note that the recovery length measured in a bad region is not expected to indicate its distance to the bifurcation point that leads to population collapse; instead it reflects the distance to re-establishment.

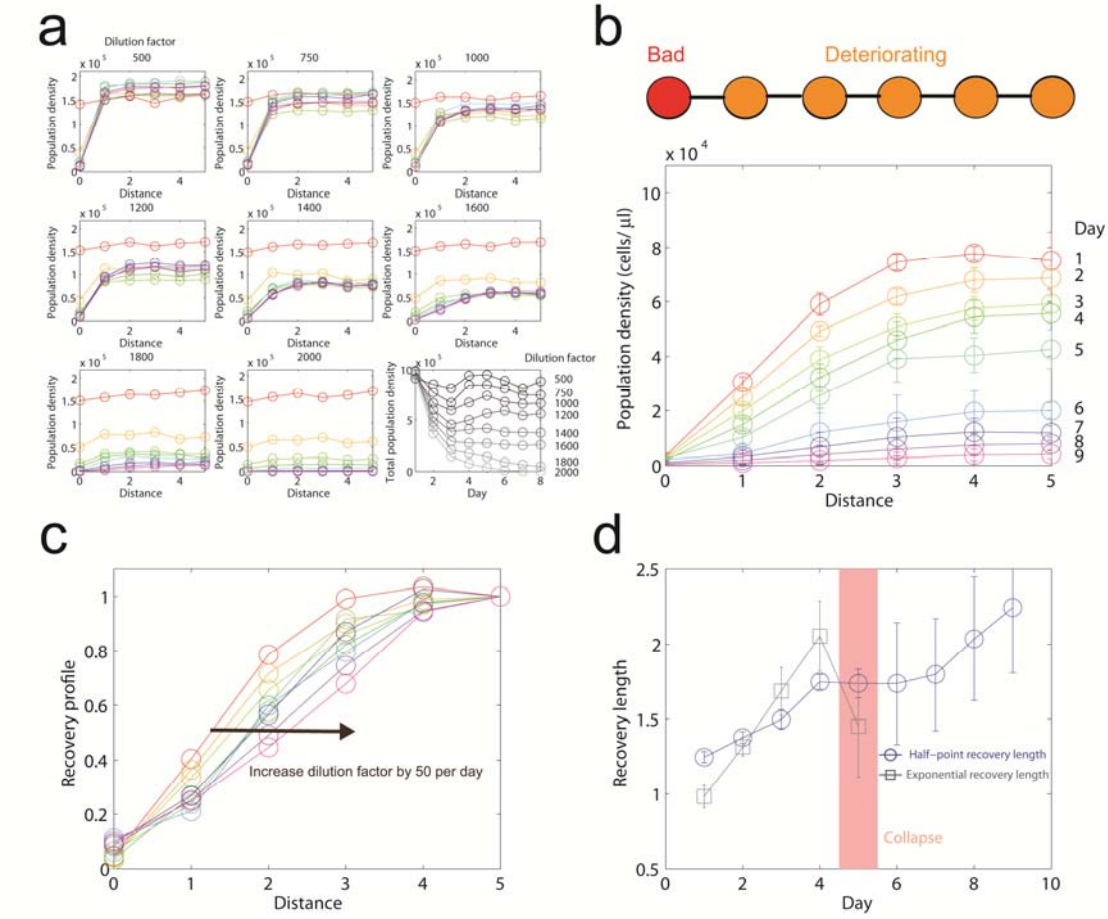

Supplementary Figure 7. Increase of recovery length before the collapse of connected populations in real time. We conducted an independent experiment to observe the increase of recovery length before population collapse in a slowly deteriorating environment. Yeast populations were connected by dispersal to nearest neighbors (D=0.5) with a bad region of 1 patch (dilution factor 2500) at the boundary. Experimental procedure is similar to the experiment in Figure 4 (Methods). (a) Profiles of the control group, which were grown at fixed conditions. The control group has a good region of 5 patches at fixed dilution factors ranging from 500 to 2000. The connected populations initially had a uniform profile (Day 1, in red) and gradually approached the steady-state profiles (Day 8, in purple). The change of total population density of 6 patches over time is plotted in the last panel. Populations survived and reached steady-state profiles up to around dilution factor 1800. We note that temperature in this experimental run was 30.0C and may have resulted in a minor shift of the tipping point.

(b) Profiles of the experimental group, which were grown in a slowly deteriorating environment. The initial profile of population density was close to the steady-state profile of dilution factor 1600 and we slowly deteriorated the good region by increasing the dilution factor by 50 per day (Supplementary Table 2). Populations started to collapse around Day 5 (dilution factor 1850), in accordance with the control group. Error bars denote standard deviation of 8 replicates. (c) The recovery profile revealed an increasing spatial scale of recovery as the environment deteriorated. The profile is averaged over replicates and normalized by the equilibrium population density, which is taken as the population density in the patch furthest from the bad region. (d) We fit the recovery profile and found an increase in two measures of recovery length before population collapse. The red line marks the estimated day (Day 5) that populations started to collapse. Error bars are SEs given by bootstrapping the 8 replicates. We were not able to obtain a reasonable confidence interval for exponential recovery length after Day 5, because the population density was low and our sample size was small (fitting became very sensitive to noise). In fact, after the tipping point is crossed recovery length is no longer a meaningful measure, because the steady-state profile is global extinction.

Supplementary Table 2. Dilution factor of the experimental group in a slowly deteriorating environment.

Day	1	2	3	4	5	6	7	8	9
Dilution factor	1650	1700	1750	1800	1850	1900	1950	2000	2050

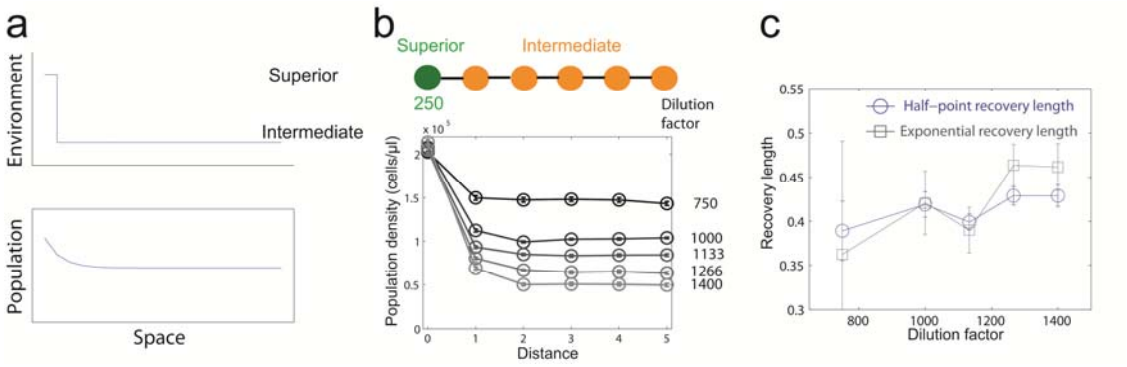

Supplementary Figure 8. Measurement of recovery length at the boundary with a region of higher quality. (a) Connected populations would gradually "recover" in space from a region of higher quality. In principle, the recovery length can be measured in this scenario (Supplementary Figure 6), suggesting that boundaries may be introduced by conservation efforts such as setting up marine reserves[36]. (b) We experimentally set up a superior patch at dilution factor 250 next to a relatively good region with varying dilution factors from 750 to 1400. Experimental procedure is similar to the experiment in Figure 4 (Methods). The steady-state profiles are shown. (c) We fit the steady-state profiles and found a modest increase in the spatial scale of recovery from a superior region. Although this spatial scale did not show a significant increase in our system, it may be a useful measure in other systems with different stability landscapes. The fitting was performed similarly to the analysis of data presented in Figure 4 (Methods). Here the position of half recovery is defined as the midpoint between the equilibrium population density and the density at the boundary $n(x = L^{half}) = \frac{1}{2}[n(x = 5) + n(x = 0)]$. The equilibrium population density was taken as the average of population density from position 3 to 5. The data points used in fitting the exponential recovery length were from position 0 to 5. Error bars are SEs given by bootstrap.

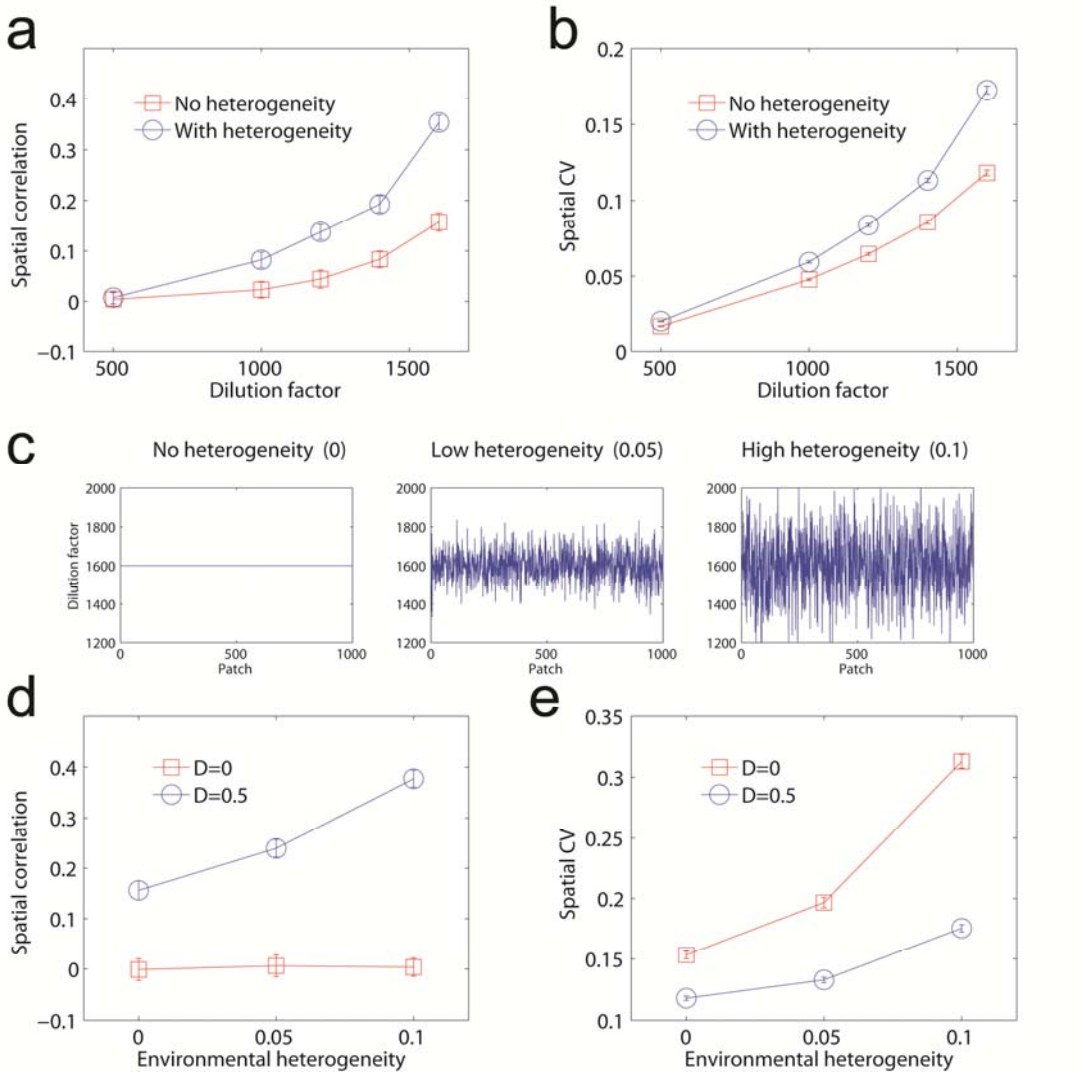

Supplementary Figure 9. Spatial statistics in the presence of environmental heterogeneity. We performed stochastic simulations based on the phenomenological model of yeast growth (Supplementary Figure 4) and introduced environmental heterogeneity by drawing the dilution factor of each patch from a Gaussian distribution $N(\mu_{DF}, \sigma_{DF}^2)$. (a, b) In the presence of heterogeneity, the signals in spatial correlation[8] and spatial variation are enhanced. The level of environmental heterogeneity $\frac{\sigma_{DF}}{\mu_{DF}}$ is set as 0 (no heterogeneity) or 0.1 (with heterogeneity). For each dilution factor, there are 1000 populations on a one-dimensional array (dispersal rate D=0.5). The indicators are averaged over a span of 5 days after an initial period of 10 days to stabilize the populations. Error bars are standard errors of 100 simulation runs. (c) We can increase the level of environmental heterogeneity by tuning the standard deviation of dilution factor. Three scenarios are shown as we vary $\frac{\sigma_{DF}}{\mu_{DF}}$ from 0 to 0.1 ($\mu_{DF} = 1600$).

(d, e) An increasing level of environmental heterogeneity could potentially lead to false alarms. At a fixed condition (dilution factor 1600), we varied $\frac{\sigma_{DF}}{\mu_{DF}}$ from 0 to 0.1 and observed increases in spatial correlation and spatial variation of connected populations (D=0.5). The isolated populations (D=0) serve as a control group: there is no spatial correlation but spatial CV is not suppressed (Supplementary Figure 4).

In our simulations, we have not explored the effect of correlations in landscape characteristics (correlated landscape)[8] or in noise (environmental correlation)[37]; they are both expected to enhance spatial correlation. In the scenario of correlated landscapes, the recovery length resulting from "islands" of different environmental quality may contribute to the increase in spatial correlation.

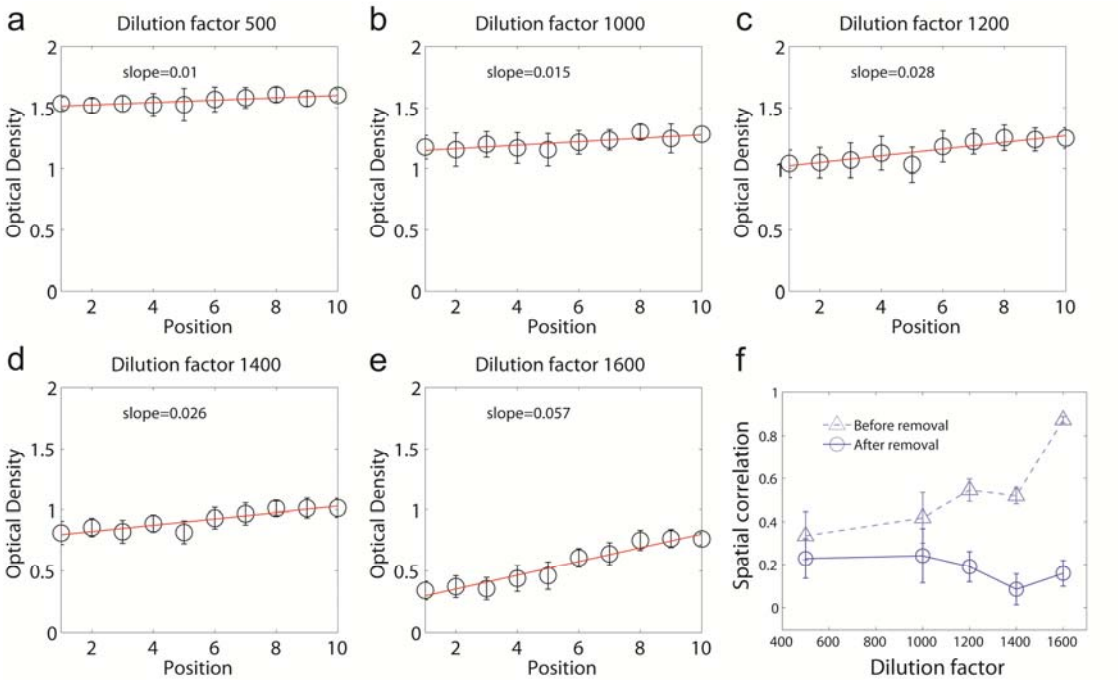

Supplementary Figure 10. A linear gradient is removed from connected populations to eliminate spurious spatial correlation. We observed a small gradient in connected populations which is presumably caused by some spatial heterogeneity in experimental conditions (temperature, dilution errors, etc.) We removed the gradient by performing a linear fit across the array. Removing gradient-type spatial heterogeneity before statistical analysis is similar to the detrending procedure commonly used in time-series analysis; it prevents spurious signals such as positive spatial correlation. (a-e) The mean optical density at each position of the array (4 replicate arrays over a span of at least 5 days), error bars are standard deviations. The red line corresponds to the linear fit. A larger slope will lead to higher spatial correlation and thus a spurious signal. (f) Spurious spatial correlation is eliminated by removing the gradient. Spatial correlation is still above 0, because there is always some level of heterogeneity in the experimental conditions. Error bars are SEMs (n=4).

Supplementary Note 1. Early warning signals in a spatially explicit first-order autoregressive model.

Critical slowing down is a generic property of dynamical systems in the vicinity of bifurcations[38,39]. Here we use a simple model to investigate warning indicators based on critical slowing down[40,41] in connected populations.

The behavior of a single isolated population in discrete time and space can be described by the following first-order autoregressive (AR(1)) process[42],

$$u_{t+1} = \rho u_t + \sigma \zeta_t \qquad (1)$$

where $u_t = n_t - n_{eq}$ is the deviation of the population density from its equilibrium value at time t; $\rho = e^{-1/T_r}$, T_r is the recovery time and indicates the distance from the bifurcation; σ is the strength of the demographic fluctuations modeled by independent Gaussian variables ζ_t (i.e. white noise).

To characterize the dynamics, we compute the statistics of an isolated population: variance $VAR_{isolated} = < u_t^2 >$ and the lag-1 autocorrelation

$AR1_{isolated} = \dfrac{< u_{t+1} u_t >}{\sqrt{< u_{t+1}^2 >< u_t^2 >}} = \dfrac{< u_{t+1} u_t >}{VAR_{isolated}}$. The bracket denotes the expectation operator which averages over realizations.

The variance is obtained by squaring both sides of equation (1), averaging over realizations, and using the time invariance of the averages (the AR(1) process is second-order stationary given $|\rho| < 1$):

$$VAR_{isolated} = \frac{\sigma^2}{1-\rho^2} \qquad (2)$$

The expression for lag-1 autocorrelation is obtained by multiplying both sides of equation (1) by u_t and averaging over realizations:

$$AR1_{isolated} = \rho \qquad (3)$$

For one-dimensional populations, the spatially explicit first-order autoregressive model takes the following form[37,43,44]

$$u_{t+1,x} = \rho[(1-D)u_{t,x} + \frac{D}{2}u_{t,x-1} + \frac{D}{2}u_{t,x+1}] + \sigma\zeta_{t,x} \qquad (4)$$

where D is the rate of dispersal; there are a total of L patches, $x = 1, 2, \ldots, L$. One can write this model in a slightly more compact form

$$\mathbf{u}_{t+1} = \rho \mathbf{M} \mathbf{u}_t + \sigma \boldsymbol{\zeta}_t \qquad (5)$$

where $\mathbf{M}$ is a $L \times L$ matrix describing dispersal. Bold symbols denote vectors, the entries being values at different patches. For example, a population of four patches with periodic boundary conditions would have the following dispersal matrix

$$\mathbf{M} = \begin{pmatrix} 1-D & \frac{D}{2} & 0 & \frac{D}{2} \\ \frac{D}{2} & 1-D & \frac{D}{2} & 0 \\ 0 & \frac{D}{2} & 1-D & \frac{D}{2} \\ \frac{D}{2} & 0 & \frac{D}{2} & 1-D \end{pmatrix} \qquad (6)$$

Note, however, that equation (5) can describe the dynamics of a population with an arbitrary dispersal pattern represented by $\mathbf{M}$ [45]. In particular, the dispersal matrix for isolated patches is the identity matrix.

In the following, we will assume: 1) $\mathbf{M}$ is positive definite (i.e. $\mathbf{u}_t^{\mathrm{T}} \mathbf{M} \mathbf{u}_t > 0$), which avoids some pathological cases like division by zero; 2) $\mathbf{u}_t^{\mathrm{T}} \mathbf{M} \mathbf{u}_t \le \mathbf{u}_t^{\mathrm{T}} \mathbf{u}_t$, which follows from the existence of a stable equilibrium and also requires the existence of an eigenvector of $\mathbf{M}$ with eigenvalue 1. For example, when $\mathbf{M}$ is symmetric and the sum of each row is 1, the first assumption is satisfied if all the diagonal elements are larger than $\frac{1}{2}$ (i.e. $D < \frac{1}{2}$); the second assumption is always satisfied and the equality sign holds for any $\mathbf{u}_t$ if and only if $\mathbf{M}$ is the identity matrix (i.e. $D = 0$). Under these assumptions, we next show that VAR and $AR1$ are suppressed in spatial populations.

Similar to the model of a single isolated population, we estimate the variance of connected populations $VAR_{connected} = \frac{< \mathbf{u}_t^{\mathrm{T}} \mathbf{u}_t >}{L}$ by squaring both sides of equation (5) and obtain

$$< \mathbf{u}_t^{\mathrm{T}} \mathbf{u}_t >= \rho^2 < \mathbf{u}_t^{\mathrm{T}} \mathbf{M}^2 \mathbf{u}_t > + \sigma^2 L \qquad (7)$$

Since $\mathbf{u}_t^{\mathrm{T}} \mathbf{M} \mathbf{u}_t \le \mathbf{u}_t^{\mathrm{T}} \mathbf{u}_t$, $\mathbf{u}_t^{\mathrm{T}} \mathbf{M}^2 \mathbf{u}_t \le \mathbf{u}_t^{\mathrm{T}} \mathbf{u}_t$, and equation (7) yields

$$VAR_{connected} \le \frac{\sigma^2}{1-\rho^2} = VAR_{isolated} \qquad (8)$$

This equation and equation (2) imply that the variance is smaller in connected populations coupled by dispersal than in isolated populations.

We can also estimate ρ by multiplying both sides of equation (5) with $\mathbf{u}_t^{\mathrm{T}}$ and averaging over realizations:

$$\rho = \frac{<\mathbf{u}_{t+1}^{\mathrm{T}}\mathbf{u}_t>}{<\mathbf{u}_t^{\mathrm{T}}\mathbf{M}\mathbf{u}_t>} \qquad (9)$$

We can readily see that $AR1$ in spatial populations is smaller than that in isolated populations because

$$AR1_{connected} = \frac{<\mathbf{u}_{t+1}^{\mathrm{T}}\mathbf{u}_t>}{\sqrt{<\mathbf{u}_{t+1}^{\mathrm{T}}\mathbf{u}_{t+1}><\mathbf{u}_t^{\mathrm{T}}\mathbf{u}_t>}} = \frac{<\mathbf{u}_{t+1}^{\mathrm{T}}\mathbf{u}_t>}{<\mathbf{u}_t^{\mathrm{T}}\mathbf{u}_t>} \le \frac{<\mathbf{u}_{t+1}^{\mathrm{T}}\mathbf{u}_t>}{<\mathbf{u}_t^{\mathrm{T}}\mathbf{M}\mathbf{u}_t>} = \rho = AR1_{isolated} \qquad (10)$$

Hence, $AR1$ are also suppressed in connected populations. Simulation results on the suppression of both indicators by dispersal are shown in Supplementary Figure 4.

When the dispersal matrix $\mathbf{M}$ is diagonalizable (e.g. $\mathbf{M}$ is symmetric), one can explicitly compute VAR and $AR1$. Upon iterating equation (5), we observe that, at a stationary state, $\mathbf{u}_t$ is given by

$$\mathbf{u}_t = \sigma\sum_{k=0}^{\infty}\rho^k\mathbf{M}^k\boldsymbol{\zeta}_{t-k-1} \quad (11)$$

The computation of moments of $\mathbf{u}_t$ is aided by the representation of $\mathbf{M}$ in terms of its eigenvectors $\mathbf{h}_j$ with unit norm and eigenvalues λ_j

$$\mathbf{M} = \sum_{j=0}^{L-1}\lambda_j\mathbf{h}_j\mathbf{h}_j^T \qquad (12)$$

The variance is then given by

$$VAR = \frac{<\mathbf{u}_t^{\mathrm{T}}\mathbf{u}_t>}{L} = \frac{\sigma^2}{L}\sum_{j=0}^{L-1}\sum_{k=0}^{\infty}\rho^{2k}\lambda_j^{2k} = \frac{\sigma^2}{L}\sum_{j=0}^{L-1}\frac{1}{1-\rho^2\lambda_j^2} \qquad (13)$$

where we used the independence of $\boldsymbol{\zeta}_t$ and the summation of an infinite decreasing geometric series.

The AR1 can be computed similarly, and the result is given by

$$AR1 = \frac{1}{VAR}\frac{\sigma^2}{L}\sum_{j=0}^{L-1}\frac{\rho\lambda_j}{1-\rho^2\lambda_j^2} \quad (14)$$

One can also compute higher order autocorrelation coefficients and show that they decay as ρ^τ for very large lag τ.

Supplementary Note 2. Recovery length in mathematical models.

When a dynamical system is closer to a tipping point, it recovers from perturbations more slowly, a phenomenon called critical slowing down. In Figure 3, we classify possible indicators of critical slowing down[1,2] based on the type of perturbations (deterministic vs. stochastic) and measurements (temporal vs. spatial). In time-series data, one can estimate the recovery time directly by measuring how long it takes for a population to recover from a pulse perturbation (Fig. 3a). In contrast, under stochastic perturbations (e.g. demographic noise), critical slowing down leads to an increase in the temporal correlation and the temporal variation (Fig. 3c). In spatially extended populations, fluctuations at different locations would allow for similar indicators based on spatial statistics, including the spatial correlation and the spatial variation (Fig.3d).

The last and unexplored category of early warning signals is the spatial counterpart of recovery time: "recovery length". The recovery length characterizes the spatial scale over which population density recovers from a pulse perturbation in space, such as at a boundary with a region of lower quality (Fig. 3b). Here we use mathematical models to demonstrate that the recovery length increases towards the tipping point and provides a novel indicator of critical slowing down in spatial data.

Half-point recovery length

We use the following continuous model of a spatial population $c(t,x)$ exhibiting the Allee effect[46] to demonstrate the half-point recovery length:

$$\frac{\partial}{\partial t}c = D\frac{\partial^2}{\partial x^2}c + gc(K-c)(c-c^*) \qquad (1)$$

In the non-spatial limit ($D=0$), the fold bifurcation occurs when the finite stable fixed point (carrying capacity) K and the unstable fixed point c^* meet, i.e. $c^* = K$.

A region of infinite mortality at $x<0$ is represented by a boundary condition $c(t,0)=0$ for equation (1). The stationary solution in this "depletion region" $c_{dep}(x)$ is obtained by setting the left hand side of equation (1) to zero, and reads

$$c_{dep}(x) = K - \frac{3K(K-c^*)}{2K-c^* + \sqrt{(\frac{K}{2}-c^*)(K+c^*)}\sinh[x\sqrt{\frac{gK(K-c^*)}{D}} + \operatorname{arcsinh}(2\sqrt{\frac{\frac{K}{2}-c^*}{K+c^*}})]} \qquad (2)$$

Upon measuring $c_{dep}(x)$ in the units of K and x in the units of $(D/gK^2)^{1/2}$, the shape of the depletion region depends only on $\frac{c^*}{K}$. This dependence is shown in Supplementary Figure 11. Note that no non-trivial solution exists when $c^* > \frac{K}{2}$.

The length of the region where $c_{dep}(x) < \frac{K}{2}$ is the half-point recovery length L^{half}.

L^{half} increases closer to the bifurcation (i.e., larger $\frac{c^*}{K}$) and diverges as $-\ln(\frac{1}{2} - \frac{c^*}{K})$.

Exponential recovery length

To derive the exponential recovery length, we start with the discrete model introduced in Supplementary Note 1. Suppose we have a steady-state recovery profile that does not change over time $u_{t+1,x} = u_{t,x} \equiv u_x$, then we have

$$u_x = \rho[(1-D)u_x + \frac{D}{2}u_{x-1} + \frac{D}{2}u_{x+1}] \quad (3)$$

We can look for a solution in the form of $u_x = \lambda^x = e^{(\ln\lambda)x}$, and solve for λ to find the characteristic spatial scale. Alternatively, closer to the equilibrium we can take the continuous limit $u_{x+1} - u_x \to \frac{d}{dx}u(x)$ and equation (3) becomes

$$\frac{d^2}{dx^2}u(x) = \frac{2(1-\rho)}{\rho D}u(x) \quad (4)$$

Given the boundary condition $u(x \to +\infty) = 0$, the non-trivial solution of equation (4) is an exponential function

$$u(x) = e^{-x/L^{\exp}}, L^{\exp} = \sqrt{\frac{2\rho D}{1-\rho}} \quad (5)$$

The exponent $L^{\exp}$ determines a characteristic spatial scale of recovery that we name as the exponential recovery length.

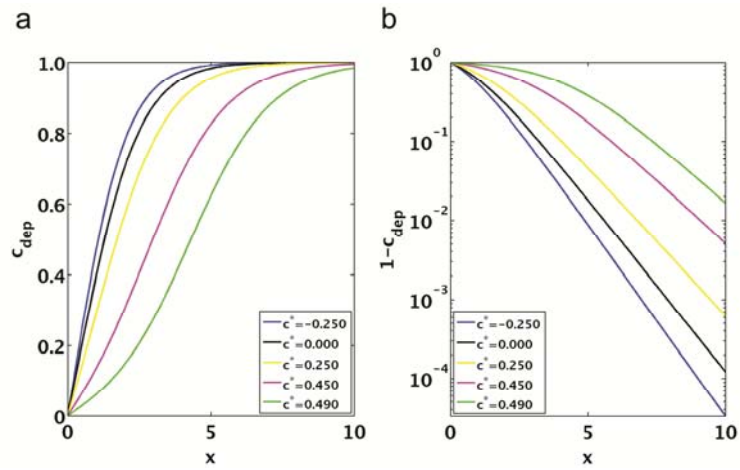

Supplementary Figure 11. Analytical solution of recovery profile in a continuous model with the Allee effect. (a)The shape of the depletion region $c_{dep}(x)$ as a function of c^*(unit: K). (b) The approach of $c_{dep}(x)$ to its limiting value at $x \to +\infty$ is approximately exponential.

Supplementary Note 3. Spatially connected populations may collapse before the tipping point of a local population.

Our experiments have not explored the effects of spatial coupling on the global stability of a meta-population[45,47]. For example, spatially extended populations subject to dispersal may require a critical patch size for survival[48,49]. Moreover, stochastic local extinctions or the introduction of a bad region can possibly drive the connected populations to collapse before the tipping point of a local population. Here we provide an example using the continuous model introduced in Supplementary Note 2,

$$\frac{\partial}{\partial t}c = D\frac{\partial^2}{\partial x^2}c + gc(K-c)(c-c^*) \qquad (1)$$

The fold bifurcation of an isolated population occurs when $c^* = K$. In a homogeneous environment, spatially coupled populations become unstable when $c^* = K$. However, in the presence of spatial heterogeneity, spatial coupling may reduce population stability. In this continuous model, populations exposed to unoccupied territories (i.e., patches with $c = 0$) will contract when $c^* > \frac{K}{2}$. This follows from the exact solution for the expansion velocity v of travelling waves[46,50]:

$$v = \sqrt{\frac{Dg}{2}}(K - 2c^*) \qquad (2)$$

when $c^* > \frac{K}{2}$, the velocity becomes negative, so the population shrinks instead of expands. The point at which $c^* = \frac{K}{2}$ is called the "Maxwell point"[51]. Thus, spatial coupling may cause populations to collapse at conditions before the bifurcation point of a local population.

In our experiments, connected populations under different setups (with or without a bad region) collapsed at relatively different conditions. This could be caused by the existence of the Maxwell point, or by other factors such as the finite patch size in our experiment and variation in experimental conditions between different experimental runs.

Supplementary Note 4. Formula of statistical indicators.

1) Sample standard deviation:

$$s = \sqrt{\frac{1}{N-1}\sum_{i=1}^{N}(n_i - < n >)^2}$$

$< n >$: the sample mean. N : total number of samples.

2) Coefficient of variation: the sample standard deviation divided by the sample mean.

3) Temporal correlation

The temporal correlation, defined as the lag-1 autocorrelation, was estimated by the Pearson's correlation coefficient between the population densities at subsequent days.

The sample Pearson's correlation coefficient:

$$\rho = \frac{1}{N-1}\frac{\sum_{i=1}^{N}(n_{t,i} - < n_t >)(n_{t+1,i} - < n_{t+1} >)}{s_t s_{t+1}}$$

$n_{t,i}$: sample i at day t; $< n_t >$: the sample mean at day t; s_t : the sample standard deviation at day t.

To correct for negative bias in small samples, we used a modified estimator with an additional term $\frac{1}{N}$ for lag-1 autocorrelation[31].

4) Spatial correlation

The spatial correlation, defined as the two-point correlation between all neighboring pairs, was estimated by the Moran's coefficient[8,32].

Moran's coefficient at day t

$$I_t = \frac{\frac{1}{W}\sum_i\sum_j w_{ij}(n_{t,i} - < n_t >)(n_{t,j} - < n_t >)}{\frac{1}{N}\sum_{i=1}^{N}(n_{t,i} - < n_t >)^2}$$

$$w_{ij} = \begin{cases} 1 & neighbors \\ 0 & others \end{cases}$$

The weight w_{ij} takes the value of 1 for nearest neighboring populations and 0 otherwise. W is the total number of neighboring pairs; $W = N - 1$ in our one-dimensional array with reflecting boundaries.

The expectation of Moran's coefficient is $-\frac{1}{N-1}$ in the absence of spatial correlation[33]; we used a modified estimator with an additional term $\frac{1}{N-1}$ so that the expectation is 0.

Supplementary References

1. Scheffer, M. *et al.* Early-warning signals for critical transitions. *Nature* **461**, 53–9 (2009).

2. Scheffer, M. *et al.* Anticipating Critical Transitions. *Science* **338**, 344–348 (2012).

3. Drake, J. M. & Griffen, B. D. Early warning signals of extinction in deteriorating environments. *Nature* **467**, 456–9 (2010).

4. Carpenter, S. R. *et al.* Early warnings of regime shifts: a whole-ecosystem experiment. *Science* **332**, 1079–82 (2011).

5. Veraart, A. J. *et al.* Recovery rates reflect distance to a tipping point in a living system. *Nature* **481**, 357–359 (2012).

6. Dai, L., Vorselen, D., Korolev, K. S. & Gore, J. Generic indicators for loss of resilience before a tipping point leading to population collapse. *Science* **336**, 1175–7 (2012).

7. Guttal, V. & Jayaprakash, C. Spatial variance and spatial skewness: leading indicators of regime shifts in spatial ecological systems. *Theor. Ecol.* **2**, 3–12 (2008).

8. Dakos, V., Nes, E. H., Donangelo, R., Fort, H. & Scheffer, M. Spatial correlation as leading indicator of catastrophic shifts. *Theor. Ecol.* **3**, 163–174 (2009).

9. Dakos, V., Kéfi, S., Rietkerk, M., Van Nes, E. H. & Scheffer, M. Slowing down in spatially patterned ecosystems at the brink of collapse. *Am. Nat.* **177**, E153–66 (2011).

10. Carpenter, S. R. & Brock, W. A. Early warnings of regime shifts in spatial dynamics using the discrete Fourier transform. *Ecosphere* **1**, art10 (2010).

11. Lindegren, M. *et al.* Early Detection of Ecosystem Regime Shifts: A Multiple Method Evaluation for Management Application. *PLoS ONE* **7**, e38410 (2012).

12. Litzow, M. A., Urban, J. D. & Laurel, B. J. Increased Spatial Variance Accompanies Reorganization of Two Continental Shelf Ecosystems. *Ecological Applications* **18**, 1331–1337 (2008).

13. Ouyang, Q. & Swinney, H. L. Transition from a uniform state to hexagonal and striped Turing patterns. *Nature* **352**, 610–612 (1991).

14. Van Nes, E. H. & Scheffer, M. Slow recovery from perturbations as a generic indicator of a nearby catastrophic shift. *Am. Nat.* **169**, 738–47 (2007).

15. May, R. M. Thresholds and breakpoints in ecosystems with a multiplicity of stable states. *Nature* **269**, 471–477 (1977).

16. Scheffer, M., Carpenter, S., Foley, J. a, Folke, C. & Walker, B. Catastrophic shifts in ecosystems. *Nature* **413**, 591–6 (2001).

17. Staver, A. C., Archibald, S. & Levin, S. A. The global extent and determinants of savanna and forest as alternative biome states. *Science* **334**, 230–2 (2011).

18. Isbell, F., Tilman, D., Polasky, S., Binder, S. & Hawthorne, P. Low biodiversity state persists two decades after cessation of nutrient enrichment. *Ecology Letters* (2013).doi:10.1111/ele.12066

19. Holling, C. S. Resilience and Stability of Ecological Systems. *Annual Review of Ecology and Systematics* **4**, 1–23 (1973).

20. Scheffer, M. *Critical transitions in nature and society*. (Princeton University Press: 2009).

21. Kleinen, T., Held, H. & Petschel-Held, G. The potential role of spectral properties in detecting thresholds in the Earth system: application to the thermohaline circulation. *Ocean Dynamics* **53**, 53–63 (2003).

22. Brock, W. A. & Carpenter, S. R. Interacting regime shifts in ecosystems: implication for early warnings. *Ecological Monographs* **80**, 353–367 (2010).

23. Boettiger, C. & Hastings, A. Early warning signals and the prosecutor's fallacy. *Proc. R. Soc. B* (2012).doi:10.1098/rspb.2012.2085

24. Rietkerk, M., Dekker, S. C., De Ruiter, P. C. & Van de Koppel, J. Self-organized patchiness and catastrophic shifts in ecosystems. *Science* **305**, 1926–9 (2004).

25. Kéfi, S. *et al.* Spatial vegetation patterns and imminent desertification in Mediterranean arid ecosystems. *Nature* **449**, 213–7 (2007).

26. Gore, J., Youk, H. & Van Oudenaarden, A. Snowdrift game dynamics and facultative cheating in yeast. *Nature* **459**, 253–6 (2009).

27. Fernández, A. & Fort, H. Catastrophic phase transitions and early warnings in a spatial ecological model. *Journal of Statistical Mechanics: Theory and Experiment* P09014 (2009).

28. Sole, R. V, Manrubia, S. C., Luque, B., Delgado, J. & Bascompte, J. Phase Transitions and Complex Systems. *Complexity* **1**, 13–26 (1996).

29. Ries, L., Fletcher, R. J., Battin, J. & Sisk, T. D. Ecological Responses To Habitat Edges: Mechanisms, Models, and Variability Explained. *Annual Review of Ecology, Evolution, and Systematics* **35**, 491–522 (2004).

30. Harper, K. A. *et al.* Edge Influence on Forest Structure and Composition in Fragmented Landscapes. *Conservation Biology* **19**, 768–782 (2005).

31. DeCarlo, L. T. & Tryon, W. W. Estimating and testing autocorrelation with small samples: A comparison of the c-statistic to a modified estimator. *Behaviour Research and Therapy* **31**, 781–788 (1993).

32. Legendre, P. & Fortin, M. J. Spatial pattern and ecological analysis. *Vegetatio* **80**, 107–138 (1989).

33. Moran, P. A. P. Notes on continuous stochastic phenomena. *Biometrika* **37**, 17–23 (1950).

34. Courchamp, F., Clutton-Brock, T. & Grenfell, B. Inverse density dependence and the Allee effect. *Trends Ecol. Evo.* **14**, 405–410 (1999).

35. Donangelo, R., Fort, H., Dakos, V., Scheffer, M. & Van Nes, E. H. Early warnings for catastrophic shifts in ecosystems: comparison between spatial and temporal indicators. *International Journal of Bifurcation and Chaos* **20**, 315–321 (2010).

36. Pauly, D. *et al.* Towards sustainability in world fisheries. *Nature* **418**, 689–95 (2002).

37. Kendall, B. E., Bjørnstad, O. N., Bascompte, J., Keitt, T. H. & Fagan, W. F. Dispersal, Environmental Correlation, and Spatial Synchrony in Population Dynamics. *The American Naturalist* **155**, 628–636 (2000).

38. Strogatz, S. H. *Nonlinear dynamics and chaos: with applications to physics, biology, chemistry, and engineering*. (Westview Press: 1994).

39. Sornette, D. *Critical Phenomena in Natural Sciences: Chaos, Fractals, Selforganization and Disorder: Concepts and Tools (Springer Series in Synergetics)*. (Springer: 2006).

40. Dakos, V. *et al.* Methods for Detecting Early Warnings of Critical Transitions in Time Series Illustrated Using Simulated Ecological Data. *PLoS ONE* **7**, e41010 (2012).

41. Carpenter, S. R. & Brock, W. A. Rising variance: a leading indicator of ecological transition. *Ecol. Lett.* **9**, 311–8 (2006).

42. Ives, A. R. Measuring Resilience in Stochastic Systems. *Ecol. Monogr.* **65**, 217-233 (1995).

43. Bascompte, J. & Solé, R. V. Rethinking complexity: modelling spatiotemporal dynamics in ecology. *Trends in Ecology & Evolution* **10**, 361–366 (1995).

44. Solé, R. V. & Bascompte, J. *Self-Organization in Complex Ecosystems*. (Princeton University Press: 2012).

45. Earn, D. J. D., Levin, S. A. & Rohani, R. Coherence and Conservation. *Science* **290**, 1360–1364 (2000).

46. Murray, J. D. *Mathematical Biology: I. An Introduction*. (Springer: 2002).

47. Hanski, I. Metapopulation dynamics. *Nature* **396**, 41–49 (1998).

48. Vercken, E., Kramer, A. M., Tobin, P. C. & Drake, J. M. Critical patch size generated by Allee effect in gypsy moth, Lymantria dispar (L.). *Ecology letters* **14**, 179–86 (2011).

49. Méndez, V. & Campos, D. Population extinction and survival in a hostile environment. *Physical Review E* **77**, 022901 (2008).

50. Lewis, M. A. & Kareiva, P. Allee Dynamics and the Spread of Invading Organisms. *Theoretical Population Biology* **43**, 141–158 (1993).

51. Bel, G., Hagberg, A. & Meron, E. Gradual regime shifts in spatially extended ecosystems. *Theoretical Ecology* (2012).